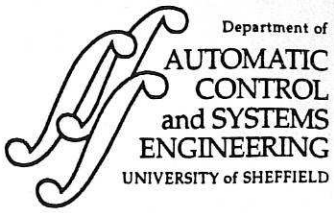

SELF-TUNING ACTIVE VIBRATION CONTROL OF FLEXIBLE BEAM STRUCTURES

M O Tokhi and M A Hossain

Department of Automatic Control and Systems Engineering, The University of Sheffield,
P O Box 600, Mappin Street, Sheffield, S1 4DU, UK.

Tel: (0742) 825136.
Fax: (0742) 731 729.
E-mail: O.Tokhi@sheffield.ac.uk.

Research Report No. 531

August 1994

Abstract

This paper presents the design and performance evaluation of an adaptive active control mechanism for vibration suppression in flexible beam structures. A cantilever beam system in transverse vibration is considered. First order central finite difference methods are used to study the behaviour of the beam and develop a suitable test and verification platform. An active vibration control algorithm is developed within an adaptive control framework for broadband cancellation of vibration along the beam using a single-input multi-output (SIMO) control structure. The algorithm is implemented on a digital processor incorporating a digital signal processing (DSP) and transputer system. Simulation results verifying the performance of the algorithm in the suppression of vibration along the beam, using single-input single-output and SIMO control structures are presented and discussed.

Key words: Active vibration control, self-tuning control, flexible beam structure.

CONTENTS

1 Introduction

Flexible structure systems are known to exhibit an inherent property of vibration when subjected to disturbance forces, leading to components and/or structural damage. Such systems include a wide range of engineering applications; for example, these in civil engineering applications include skyscrapers and bridges, in aerospace structures include propellers, aircraft fuselage and wings, satellite solar panels and helicopter blades and in electro-mechanical systems include turbogenerator shafts, engines, gas turbine rotors and electric transformer cores. An understanding of the principles involved in the analysis of such systems is important so that suitable control laws for effective suppression of undesirable vibrations can be developed.

Many attempts have been made in the past at devising methods of tackling the problems arising due to unwanted structural vibrations (disturbances). Traditional methods of vibration suppression include passive methods which consist of mounting passive material on the structure. These methods are efficient at high frequencies but expensive and bulky at low frequencies. Moreover, the current trend towards light-weight, hence flexible, structures has imposed a further limitation to the utilisation of passive methods, specially for low-frequency vibration suppression. Active vibration control (AVC) uses the superposition of waves by artificially generating secondary (cancelling) source(s) of vibration to destructively interfere with unwanted disturbances and thus result in cancellation of the unwanted vibrations. This is found to be more efficient and economical than passive methods at low-frequency vibration suppression. Thus, to achieve vibration suppression over the full (low-high) frequency range, a hybrid control method incorporating active techniques for low-frequency and passive techniques for high-frequency vibration suppression can be utilised (Leitch and Tokhi, 1987; Tokhi and Leitch, 1991a).

Active vibration control is not a new concept. It is based on the principles that were initially proposed by Lueg in the early 1930s for noise cancellation (Lueg, 1936). Since then a considerable amount of research work has been devoted to the development of

methodologies for the design and realisation of AVC systems in various applications (Baz and Poh, 1988; Baz and Ro, 1991; Baz et.al, 1990a,b; Burton, 1993; Firoozian and Stanway, 1988; Jayasuriya and Chopra, 1990; Kourmoulis, 1990; Krishnamurthy and Chao, 1992; Lu et.al, 1989; Tanaka and Kikushima, 1988; Tzou and Gadre, 1990; Yaniv and Horowitz, 1990). An AVC system is realised by detecting the primary (unwanted) disturbances through detection sensor(s) and processing these by an electronic controller of suitable transfer characteristics to drive the secondary source(s) (actuators) so that when the secondary wave is superimposed on the primary wave the two destructively interfere with one another and cancellation occurs. Active vibration control mechanisms developed generally concentrate on reducing the level of vibrations at selective resonance modes of the system. In doing so, problems related to observation and/or control spill-over due to un-modelled dynamics of the system arise. These problems can be avoided by designing an AVC system that incorporates a suitable system identification algorithm through which an appropriate model of the system can be developed within the frequency range of interest. The AVC system presented in this paper includes an on-line system identification algorithm which gives a suitable model of the system in parametric form within a broad range of frequencies of interest. The model thus obtained is then used to design the required controller and generate the corresponding control signal so that to reduce the level of vibration over this broad frequency range.

It is important to note that, the superposition of the component waves in an AVC system results in an interference pattern throughout the structure in which the level of cancellation in some regions will be higher and in some regions it will be lower or even will correspond to a reinforcement. The level and physical extent of cancellation achieved is primarily dependent on the geometrical arrangement of system components. Moreover, the number of secondary sources, depending on limitations due to physical dimensions, has a significant effect on the level as well as physical extent of cancellation.

Due to the broadband nature of the disturbances, it is required that the control mechanism in an AVC system realises suitable frequency-dependent characteristics so that cancellation over a broad range of frequencies is achieved. Moreover, in practice, the

spectral contents of the disturbances as well as the characteristics of system components are, in general, subject to variation, giving rise to time-varying phenomena. This implies that the control mechanism is further required to be intelligent enough to track these vibrations so that the desired level of performance is achieved and maintained (Tokhi and Leitch, 1991a; Tokhi et.al, 1992).

A cantilever beam system in transverse vibration is considered in this paper. Such a system has an infinite number of modes although in most cases the lower modes are the dominant ones requiring attention. The unwanted vibrations in the structure are assumed to be due to a single point disturbance of broadband nature. First order central finite difference (FD) methods are used to study the behaviour of the beam and develop a suitable test and verification platform. An AVC system is designed utilising a single-input multi-output (SIMO) control structure to yield optimum cancellation of broadband vibration at a set of observation points along the beam. The controller design relations are formulated such that to allow on-line design and implementation and, thus, yield a self-tuning control algorithm. The algorithm is implemented on a parallel heterogeneous system incorporating a DSP device and a transputer node and its performance assessed in the suppression of vibration along the beam using single-input single-output (SISO) and SIMO control structures.

2 The cantilever beam system

A schematic diagram of the cantilever beam system is shown in Figure 1, where L represents the length of the beam, $U(x,t)$ represents an applied force at a distance x from the fixed (clamped) end of the beam at time t and $y(x,t)$ is the deflection of the beam from its stationary (unmoved) position at the point where the force has been applied. The motion of the beam in transverse vibration is governed by the well known fourth-order partial differential equation (PDE) (Virk and Kourmoulis, 1988)

$$\mu^2 \frac{\partial^4 y(x,t)}{\partial x^4} + \frac{\partial^2 y(x,t)}{\partial t^2} = \frac{1}{m} U(x,t) \tag{1}$$

where μ is a beam constant given by $\mu^2 = \frac{EI}{\rho A}$, with ρ, A, I and E representing the mass density, cross-sectional area, moment of inertia of the beam and the Young's modulus respectively, and m is the mass of the beam. The corresponding boundary conditions at the fixed and free ends of the beam are given by

$$\begin{aligned} y(0,t) = 0 \quad \text{and} \quad \frac{\partial y(0,t)}{\partial x} = 0 \\ \frac{\partial^2 y(L,t)}{\partial x^2} = 0 \quad \text{and} \quad \frac{\partial^3 y(L,t)}{\partial x^3} = 0 \end{aligned} \tag{2}$$

Note that the model thus utilised incorporates no damping. To construct a suitable platform for test and verification of the control mechanism (introduced later), a method of obtaining numerical solution of the PDE in equation (1) is required. The finite element (FE) method has commonly been used in the past for obtaining numerical solutions of the PDE and for constructing simulation environments characterising the behaviour of such systems (Chen and Ku, 1990; Lin and Trethewey, 1990; Tzou and Tseng, 1990; Udupa and Varadan, 1990). This method allows irregularities in the structure and mixed boundary conditions to be handled. However, these are not of concern in the case of a uniform beam structure considered here. Moreover, the computational effort and consequent software coding involved in the FE method makes it unfavourable for uniform structures. It has been reported that the FD method is more suitable in the simulation of uniform beam structures and simpler than the FE method (Kourmoulis, 1990). For the system considered here, the dynamics may efficiently be described in terms of a modal expansion. However, a virtue of the FD method is that it could fairly readily be applied to more complicated mechanical systems, for which an analytic modal solution could not be readily obtained. Therefore, the FD method is used here for obtaining a numerical solution of the PDE in

equation (1) and for constructing a suitable simulation environment characterising the behaviour of the beam.

To obtain a solution to the PDE, describing the beam motion, the partial derivative terms $\frac{\partial^4 y(x,t)}{\partial x^4}$ and $\frac{\partial^2 y(x,t)}{\partial x^2}$ in equation (1) and the boundary conditions in equation (2) are approximated using first order central FD approximations. This involves a descretisation of the beam into a finite number of equal-length sections (segments), each of length Δx, and considering the beam motion (deflection) for the end of each section at equally-spaced time steps of duration Δt. In this manner, let $y(x,t)$ be denoted by $y_{i,j}$ representing the beam deflection at point i at time step j. Let $y(x+v\Delta x, t+w\Delta t)$ be denoted by $y_{i+v,j+w}$, where v and w are non-negative integer numbers.

Using a first-order central FD method the partial derivatives $\frac{\partial^2 y}{\partial t^2}$ and $\frac{\partial^4 y}{\partial x^4}$ can be approximated as

$$\frac{\partial^2 y(x,t)}{\partial t^2} = \frac{y_{i,j+1} - 2y_{i,j} + y_{i,j-1}}{(\Delta t)^2}$$
$$\frac{\partial^4 y(x,t)}{\partial x^4} = \frac{y_{i+2,j} - 4y_{i+1,j} + 6y_{i,j} - 4y_{i-1,j} + y_{i-2,j}}{(\Delta x)^4} \qquad (3)$$

Substituting for $\frac{\partial^2 y}{\partial t^2}$ and $\frac{\partial^4 y}{\partial x^4}$ from equation (3) into equation (1) and simplifying yields

$$y_{i,j+1} = 2y_{i,j} - y_{i,j-1} - \lambda^2\{y_{i+2,j} - 4y_{i+1,j} + 6y_{i,j} - 4y_{i-1,j} + y_{i-2,j}\} + \frac{(\Delta t)^2}{m}U(x,t) \qquad (4)$$

where, $\lambda^2 = \frac{(\Delta t)^2}{(\Delta x)^4}\mu^2$. Equation (4) gives the deflection of point i along the beam at time step $j+1$ in terms of the deflections of the point at time steps j and $j-1$ and deflections of points $i-1$, $i-2$, $i+1$ and $i+2$ at time step j. Note that in evaluating the deflection at the grid point $i=1$ the fictitious deflection $y_{-1,j}$ will be required. Similarly, in evaluating the deflection at the free end of the beam, $i=n$ (n representing the total number of

sections along the beam), the fictitious deflections $y_{n+1,j}$ and $y_{n+2,j}$ will be required. To obtain these, the boundary conditions in equation (2) are used. In a similar manner as above, the boundary conditions in equation (2) can be expressed in terms of the FD approximations as

$$\begin{aligned} y_{0,j} &= 0 \quad , \quad \frac{y_{1,j} - y_{-1,j}}{2\Delta x} = 0 \\ \frac{y_{n+1,j} - 2y_{n,j} + y_{n-1,j}}{(\Delta x)^2} &= 0 \quad , \quad \frac{y_{n+2,j} - 2y_{n+1,j} + 2y_{n-1,j} - y_{n-2,j}}{2(\Delta x)^3} = 0 \end{aligned} \tag{5}$$

Solving equation (5) for the deflections $y_{-1,j}$ and $y_{0,j}$ at the fixed end and $y_{n+1,j}$ and $y_{n+2,j}$ at the free end yields

$$\begin{aligned} y_{0,j} &= 0 \quad \text{and} \quad y_{-1,j} = y_{1,j} \\ y_{n+1,j} &= 2y_{n,j} - y_{n-1,j} \quad \text{and} \quad y_{n+2,j} = 2y_{n+1,j} - 2y_{n-1,j} + y_{n-2,j} \end{aligned} \tag{6}$$

Equations (4) and (6) give the complete set of relations necessary for the construction of the simulation algorithm. Substituting the discretised boundary conditions for the fixed and free ends from equations (6) into equation (4) yield the beam deflection at the grid points along the beam as

$$\begin{aligned} y_{1,j+1} &= -y_{1,j-1} - \lambda^2\{(7 - \frac{2}{\lambda^2})y_{1,j} - 4y_{2,j} + y_{3,j}\} + \phi \\ y_{2,j+1} &= -y_{2,j-1} - \lambda^2\{-4y_{1,j} + (6 - \frac{2}{\lambda^2})y_{2,j} - 4y_{3,j} + y_{4,j}\} + \phi \\ &\vdots \\ y_{n,j+1} &= -y_{n,j-1} - \lambda^2\{2y_{n-2,j} + -4y_{n-1,j} + (2 - \frac{2}{\lambda^2})y_{n,j}\} + \phi \end{aligned}$$

where, $\phi = \dfrac{(\Delta t)^2}{m} U(x,t)$. The above equations can be written in a matrix form as

$$Y_{j+1} = -Y_{j-1} - \lambda^2 S Y_j + (\Delta t)^2 U(x,t)\frac{1}{m} \tag{7}$$

where,

$$Y_{j+1} = \begin{bmatrix} y_{1,j+1} \\ y_{2,j+1} \\ \vdots \\ y_{n,j+1} \end{bmatrix}, \quad Y_j = \begin{bmatrix} y_{1,j} \\ y_{2,j} \\ \vdots \\ y_{n,j} \end{bmatrix}, \quad Y_{j-1} = \begin{bmatrix} y_{1,j-1} \\ y_{2,j-1} \\ \vdots \\ y_{n,j-1} \end{bmatrix},$$

and S is a matrix given (for $n = 19$, say) as

$$S = \begin{bmatrix} a & -4 & 1 & 0 & 0 & 0 & \cdots & \cdots & 0 \\ -4 & b & -4 & 1 & 0 & 0 & \cdots & \cdots & 0 \\ 1 & -4 & b & -4 & 1 & 0 & \cdots & \cdots & 0 \\ 0 & 1 & -4 & b & -4 & 1 & \cdots & \cdots & 0 \\ \cdots & \cdots & \cdots & \cdots & \cdots & \cdots & \cdots & \cdots & \cdots \\ \cdots & \cdots & \cdots & \cdots & \cdots & \cdots & \cdots & \cdots & \cdots \\ \cdots & \cdots & \cdots & \cdots & 1 & -4 & b & -4 & 1 \\ \cdots & \cdots & \cdots & \cdots & 0 & 1 & -4 & c & -2 \\ \cdots & \cdots & \cdots & \cdots & 0 & 0 & 2 & -4 & d \end{bmatrix}$$

where, $a = 7 - \frac{2}{\lambda^2}$, $b = 6 - \frac{2}{\lambda^2}$, $c = 5 - \frac{2}{\lambda^2}$ and $d = 2 - \frac{2}{\lambda^2}$. Equation (7) is the required relation for the simulation algorithm, characterising the behaviour of the cantilever beam system, which can be implemented on a digital computer easily. For the algorithm to be stable it is required that the iterative scheme described in equation (7), for each grid point, converges to a solution. It has been shown that a necessary and sufficient condition for stability satisfying this convergence requirement is given by $0 < \lambda^2 \leq 0.25$ (Kourmoulis, 1990).

To investigate the real-time implementation of the simulation algorithm and study the behaviour of the system an aluminium type cantilever beam of length *L=0.635* m; mass *m=0.037 Kg* and μ *=1.351* was considered. The first five resonance modes of this beam, as obtained through theoretical analysis, are located at *1.875* Hz, *11.751* Hz, *32.902* Hz, *64.476* Hz and *106.583* Hz respectively with the first two modes dominantly representing

the behaviour of the beam. It was found through numerical simulations that for the purpose of this investigation reasonable accuracy in representing the first few (dominant) modes of vibration is achieved by dividing the beam into 19 segments ($n = 19$). Therefore, $n = 19$ was chosen throughout the investigations presented in this paper. Moreover, sample period $\Delta t = 0.3$ *msec* which is sufficient to cover all the resonance modes of vibration of the beam was selected. For the algorithm to be stable, this gives a value of $\lambda = 0.3629$.

The behaviour of the beam in transverse vibration was studied by implementing the simulation algorithm in real-time on a digital computing system incorporating an i860 DSP device and a T805 transputer. The computing system utilised is to provide more accurate and efficient implementation of the simulation and control algorithms investigated in this paper. Although in simulation experiments the speed of implementation of the processes involved is not of major concern and thus a general purpose digital computing facility could be utilised instead, in practical investigations, however, it is essential for the computing system to meet the real-time processing requirements of the algorithm(s) involved.

Figure 2 shows the end point response of the cantilever beam due to the application of a step disturbance force of finite-duration of $0.1N$ at grid point 15. The corresponding spectral density of the response is shown in Figure 3. The first five resonance modes, as obtained from these results, are located at *2* Hz, *11* Hz, *30* Hz, *57* Hz and *91* Hz respectively. These, as compared with the corresponding theoretical values, are within reasonably acceptable limits. It is seen in Figures 2 and 3 that the first resonance mode is much more dominant than the rest. Therefore, substantial reduction in the overall level of vibration will be achieved if the first mode is cancelled by a vibration control system. Note in Figure 2 that the first mode of vibration appears to be dominantly characterising the beam fluctuation. The second and higher modes, although present in the description (Figure 3), are not as clearly evident. In general, two factors, namely, the nature of the disturbance including its amplitude and frequency contents and the location at which it is applied determine the dynamic modes of the structure that are excited and the level at

which these modes will appear. A Three-dimensional description of the vibration of the beam along its length due to the application of the step disturbance force at grid point 15 is shown in Figure 4. This shows that the beam deflection is zero at the fixed end and increases with the distance x from the fixed end, reaching a maximum at the free end, verifying the validity of the simulation algorithm in representing the behaviour of the beam.

3 Active vibration control structure

A schematic diagram of the geometric arrangement of a feedforward SIMO AVC structure is shown in Figure 5(a). A primary (disturbance) force is applied by a point source at a point along the beam. This is detected by a detector (sensor), processed by a controller of suitable frequency-dependent characteristics and fed to a set of k secondary sources (control actuators). The control force thus generated interferes with the disturbance force so that to achieve a reduction in the level of vibration at a set of k observation points along the beam.

A frequency-domain equivalent block diagram of the AVC structure is shown in Figure 5(b), where, $\mathbf{E} = [e]$ is a 1×1 matrix representing the transfer characteristics of the path along the beam between the primary source and the detector, $\mathbf{F}$ is a $k\times1$ matrix representing the transfer characteristics of the paths along the beam from the secondary sources to the detection point, $\mathbf{G}$ is a $1\times k$ matrix representing the transfer characteristics of the paths along the beam from the primary source to the observation points, $\mathbf{H}$ is a $k\times k$ matrix representing the transfer characteristics of the paths along the beam from the secondary sources to the observation points, $\mathbf{M}$ is a 1×1 matrix representing the transfer characteristics of the detector, $\mathbf{M}_o$ is a $k\times k$ diagonal matrix representing the transfer characteristics of the observers, $\mathbf{L}$ is a $k\times k$ diagonal matrix representing the transfer characteristics of the secondary sources and $\mathbf{C}$ is a $1\times k$ matrix representing the transfer characteristics of the controller;

$$\mathbf{F}=\begin{bmatrix} f_1 & f_2 & \cdots & f_k \end{bmatrix}^T \qquad \mathbf{G}=\begin{bmatrix} g_1 & g_2 & \cdots & g_k \end{bmatrix}, \quad \mathbf{H}=\begin{bmatrix} h_{11} & h_{12} & \cdots & h_{1k} \\ h_{21} & h_{22} & \cdots & h_{2k} \\ \vdots & \vdots & \vdots & \vdots \\ h_{k1} & h_{k2} & \cdots & h_{kk} \end{bmatrix} \tag{8}$$

$$\mathbf{M}_o=\begin{bmatrix} m_{o1} & 0 & \cdots & 0 \\ 0 & m_{o2} & \cdots & 0 \\ \vdots & \vdots & \vdots & \vdots \\ 0 & 0 & \cdots & m_{ok} \end{bmatrix}, \quad \mathbf{L}=\begin{bmatrix} l_1 & 0 & \cdots & 0 \\ 0 & l_2 & \cdots & 0 \\ \vdots & \vdots & \vdots & \vdots \\ 0 & 0 & \cdots & l_k \end{bmatrix}$$

$$\mathbf{C}=\begin{bmatrix} c_1 & c_2 & \cdots & c_k \end{bmatrix}$$

$\mathbf{U}_D$ is a 1×1 matrix representing the disturbance (primary) signal at the source, $\mathbf{Y}_{OD}$ is a $1\times k$ matrix representing the disturbance signals at the observation points, $\mathbf{U}_C$ is a $1\times k$ matrix representing the control (secondary) signals at the source, $\mathbf{Y}_{OC}$ is a $1\times k$ matrix representing the control signals at the observation points, $\mathbf{U}_M$ is a 1×1 matrix representing the detected signal and $\mathbf{Y}_O$ is a $1\times k$ matrix representing the observed signals.

The block diagram in Figure 5 can be thought either in the continuous complex frequency, s, domain or in the discrete complex frequency, z, domain. The analysis and design presented in this paper apply equally to both domains. The implementation of the controller, however, is carried out in the discrete-time domain.

The objective in Figure 5 is to achieve full (optimum) vibration suppression at the observation points. This is equivalent to the minimum variance design criterion in a stochastic environment. This requires the primary and secondary signals at each observation point to be equal in amplitudes and have a phase difference of 180^0 relative to one another;

$$\mathbf{Y}_O=(\mathbf{Y}_{OD}+\mathbf{Y}_{OC})\mathbf{M}_o=0 \tag{9}$$

Using the block diagram of Figure 5(b) the signals $\mathbf{Y}_{OD}$ and $\mathbf{Y}_{OC}$ can be obtained as

$$\mathbf{Y}_{OD} = \mathbf{U}_D\mathbf{G}$$
$$\mathbf{Y}_{OC} = \mathbf{U}_D\mathbf{EGMCL}[\mathbf{I}-\mathbf{FMCL}]^{-1}\mathbf{H} \tag{10}$$

Where $\mathbf{I}$ is the identity matrix. Substituting for $\mathbf{Y}_{OD}$ and $\mathbf{Y}_{OC}$ from equation (10) into equation (9) and solving for $\mathbf{C}$ yields

$$\mathbf{C} = \mathbf{M}^{-1}\left[\mathbf{GH}^{-1}\mathbf{F}-\mathbf{E}\right]^{-1}\mathbf{GH}^{-1}\mathbf{L}^{-1} \tag{11}$$

Equation (11) is the required controller transfer function for optimum suppression of broadband vibration at the observation points. The controller thus designed is assured to be causal by making the number of zeros in each path either equal to or less than the number of poles accordingly. Note that, for given secondary sources and detection sensor the characteristics of the required controller are determined by the geometric arrangement of system components. Among these, it is possible with some arrangements that the determinant $\left|\mathbf{GH}^{-1}\mathbf{F}-\mathbf{E}\right|$ will be zero or close to zero, requiring the controller to have impractically large gains. Moreover, with some geometrical arrangements of system components, the (positive) feedback loops due to the secondary signals reaching the detection point can cause the system to become unstable. Therefore, for the system performance to be robust, a consideration of the system in relation to the geometric arrangement of system components is important at a design stage (Tokhi and Leitch, 1991b).

The controller transfer function in equation (11) can be realised either as a fixed digital or analogue or hybrid (combined analogue and digital) controller through a process of measurement/estimation of the transfer characteristics of the propagation paths along the beam and through the sensor and actuators to allow design and implementation of the controller according to equation (11). In practice, the characteristics of sources of disturbance vary due to operating conditions, for instance, leading to time-varying spectra. Moreover, the characteristics of transducers, sensors and other electronic equipment used

in the AVC system are subject to variation due to environmental effects, ageing, etc. Under such situations the system employing a fixed controller will not perform to a desired level. Thus, under such circumstances an AVC system is required to be capable of updating the controller characteristics in accordance with the changes in the system so that the required level of performance is achieved and maintained. To do this a self-tuning control strategy, allowing on-line design and implementation of the controller, can be utilised.

4 Self-tuning active vibration control

The design relation given for the controller transfer function in equation (11) is in a form that is not suitable for on-line implementation. To allow on-line design and implementation of the controller, equivalent design rules based on on-line measurement of (input/output) signals of the system are required. To devise such a strategy, a self-tuning control mechanism is developed.

Self-tuning control is distinguished as a class of adaptive control mechanisms (Harris and Hillings, 1981; Tokhi and Leitch, 1992; Wellstead and Zarrop, 1991). It essentially consists of the processes of identification and control, both implemented on-line. The identification process is mainly concerned with on-line modelling of the plant to be controlled and, thus, incorporates a suitable system identification algorithm. The control process, on the other hand, is concerned with the design and implementation of the controller using the plant model and, thus, incorporates a suitable controller design criterion. In this manner, various types of self-tuning control algorithm can be designed depending on the type of the identification algorithm and controller design strategy employed. Many system identification schemes have been used in self-tuning control algorithms. Among these, the recursive form of the least squares algorithm which produces unbiased estimates of a plant model (in parametric form), based on measurements of the input and output signals of the plant, has proved to be the most useful and practically successful self-tuning identifier. In a similar manner, several controller design criteria have

been used in self-tuning control algorithms. Among these, the most common ones are the minimum variance and pole assignment designs. A self-tuning control algorithm can either be designed as an explicit combination of identification of a plant model and controller design or as an implicit algorithm in which the controller is identified directly (bypassing identification of the plant model). Each of these algorithms have their advantages and disadvantages which depend mainly on the type of application and availability of resources for implementation. Self-tuning is, in a sense, the simplest possible adaptive control algorithm derivable from the point of view of the discrete-time stochastic control theory. An attractive property of the self-tuning controller is that under most reasonable circumstances, as the number of input and output samples tends to infinity, it will converge to the optimal controller that would be obtained if the system parameters are exactly known. Moreover, the strategy is simple enough to allow the use of digital processors for implementing self-tuning controllers, thus promising a relatively low cost solution to complex control problems. In this paper an explicit self-tuning AVC algorithm, incorporating a recursive least squares (RLS) parameter estimation algorithm and the minimum variance design criterion, is developed.

To develop the self-tuning AVC system, consider Figure 5 with measurable input and output signals as the detected signal $\mathbf{U}_M$ and the observed signal $\mathbf{Y}_O$ respectively. Thus, owing to the state of each secondary source, a model of the system between the detection point and each observation point can be obtained. This will result in a set of models with equivalent transfer functions denoted by q_{oj} ($j = 1, 2, ...,k$) when all the secondary sources are *off* and a further set of models with equivalent transfer functions denoted by q_{ij} when all the secondary sources are off except secondary source i. In this manner, a total of $k(k+1)$ models can be constructed.

From the block diagram in Figure 5(b) the detected signal $\mathbf{U}_M$ and the observed signal $\mathbf{Y}_O$ can be obtained as

$$\mathbf{U}_M = \mathbf{U}_D\mathbf{EM}(\mathbf{I}-\mathbf{CLFM})^{-1}$$
$$\mathbf{Y}_O = \mathbf{U}_D\{\mathbf{G}+\mathbf{EMCL}(\mathbf{I}-\mathbf{FMCL})^{-1}\mathbf{H}\}\mathbf{M}_O \tag{12}$$

Thus, the equivalent transfer functions of system's models, for the corresponding situation under consideration, is given by the ratio $\mathbf{Y}_O\mathbf{U}_M^{-1}$ in equation (12).

Substituting for **E**, **F**, **G**, **H**, **L** and **C** from equation (8) into equation (11) and simplifying yields a relation for each element of **C** as

$$c_i = \frac{1}{b_i}\frac{\sum_{j=1}^{k} g_j H_{ij}}{\sum_{i=1}^{k} f_i\left(\sum_{j=1}^{k} g_j H_{ij}\right) - e|\mathbf{H}|}; \quad i = 1,2,\ldots,k \tag{13}$$

where c_i is the ith element of **C**, $b_i = \mathbf{M}l_i$ with l_i representing the transfer characteristics of secondary source i, g_j represents the transfer characteristics of the path, along the beam, between the primary source and observation point j,

$$H_{ij} = (-1)^{i+j}\begin{vmatrix} h_{11} & h_{12} & \cdots & h_{1(j-1)} & h_{1(j+1)} & \cdots & h_{1k} \\ h_{21} & h_{22} & \cdots & h_{2(j-1)} & h_{2(j+1)} & \cdots & h_{2k} \\ \vdots & \vdots & \vdots & \vdots & \vdots & \vdots & \vdots \\ h_{(i-1)1} & h_{(i-1)2} & \cdots & h_{(i-1)(j-1)} & h_{(i-1)(j+1)} & \cdots & h_{(i-1)k} \\ h_{(i+1)1} & h_{(i+1)2} & \cdots & h_{(i+1)(j-1)} & h_{(i+1)(j+1)} & \cdots & h_{(i+1)k} \\ \vdots & \vdots & \vdots & \vdots & \vdots & \cdots & \vdots \\ h_{k1} & h_{k2} & \cdots & h_{k(j-1)} & h_{k(j+1)} & \cdots & h_{kk} \end{vmatrix}$$

with h_{ij} representing the transfer characteristics of the path, along the beam, between secondary source i and observation point j and $|\mathbf{H}|$ represents the determinant of the matrix **H**.

To obtain c_i in equation (13) in terms of the transfer functions of system models, two cases, namely, when all secondary sources are *off* and when only secondary source i is *on*, are considered (the primary source is *on* throughout).

(1) To switch *off* all secondary sources the 'controller' in Figure 5(a) can be replaced with an 'open' switch. This in terms of the block diagram in Figure 5(b) is equivalent to all entries in **C** initialised to zero;

$$\mathbf{C}=[0 \quad 0 \quad \cdots \quad 0] \tag{14}$$

Substituting for **C** from equation (14) into equation (12) and simplifying yields the equivalent transfer functions q_{oj} ($j=1, 2, ..., k$) as

$$q_{oj}=\frac{m_{oj}g_i}{\mathbf{M}e}, \quad j=1,2,\ldots,k \tag{15}$$

where m_{oj} is the transfer function of observer j.

(2) To keep only secondary source i *on* the 'controller' in Figure 5(a) can be represented by a switch in which only the path through to secondary source i is closed. This in terms of the block diagram in Figure 5(b) is equivalent to the matrix **C** initialised to unity at location i and to zero in all other locations;

$$\mathbf{C}=[0 \quad \cdots \quad 0 \quad 1 \quad 0 \quad \cdots \quad 0] \tag{16}$$

Note in equation (16) that, for simplicity purposes, element i of the controller is initialised to unity in this case. The procedure given below equally applies to the general situation where the path from the detector to secondary source i is closed through an electronic component of a particular transfer function. In this case, element i of the controller in equation (16) can be replaced by this (initial) transfer function and thus carried throughout the synthesis process. It must be noted, however, that this initial transfer function should be included within the AVC system in cascade with the required controller transfer function during the implementation process. Note that the feedback loop formed through secondary source i to the detector by switching on the corresponding controller path may

cause the system to become unstable. Under such a situation the choice of utilising an initial transfer function instead of the switch to bring the loop gain below unity and thus allow the system to be stable during the identification phase will be favoured.

Substituting for **C** from equation (16) into equation (12), simplifying and using equation (15) yields

$$q_{ij} = q_{oj}\left[\left(\frac{h_{ij}e}{g_j} - f_i\right)b_i + 1\right]$$

or

$$\left(\frac{h_{ij}e}{g_j} - f_i\right)b_i = \frac{q_{ij}}{q_{oj}} - 1; \quad i = 1,2,\ldots,k \quad \text{and} \quad j = 1,2,\ldots,k \tag{17}$$

Adding the relations for $i = 1$ to k in equation (17) yields

$$\sum_{i=1}^{k}\left(\frac{h_{ij}e}{g_j} - f_i\right)b_i = \frac{1}{q_{oj}}\sum_{i=1}^{k} q_{ij} - k; \qquad j = 1,2,\ldots.k \tag{18}$$

Equation (18) corresponds to the system description in Figure 5 when all the secondary sources are switched on; i.e. all entries in the matrix **C** initialised to unity. Solving equation (18) for b_i $(i = 1,2,\ldots,k)$, manipulating each and using equation (13) yields

$$\frac{1}{c_i} = 1 - \frac{1}{W_i}\left\{\sum_{j=1}^{k}\frac{g_j V_{ij}}{q_{oj}}\left(\sum_{p=1}^{k} q_{pj} - k + 1\right)\right\}; \quad i = 1,2,\ldots,k \tag{19}$$

where,

$$V_{ij} = (-1)^{i+j} \begin{vmatrix} e & f_1 & \cdots & f_{(i-1)} & f_{(i+1)} & \cdots & f_k \\ g_i & h_{11} & \cdots & h_{(i-1)1} & h_{(i+1)1} & \cdots & h_{k1} \\ \vdots & \vdots & \vdots & \vdots & \vdots & \vdots & \vdots \\ g_{j-1} & h_{1(j-1)} & \cdots & h_{(i-1)(j-1)} & h_{(i+1)(j-1)} & \cdots & h_{k(j-1)} \\ g_{(j+1)} & h_{1(j+1)} & \cdots & h_{(i-1)(j+1)} & h_{(i+1)(j+1)} & \cdots & h_{k(j+1)} \\ \vdots & \vdots & \vdots & \vdots & \vdots & \vdots & \vdots \\ g_k & h_{1k} & \cdots & h_{(i-1)k} & h_{(i+1)k} & \cdots & h_{kk} \end{vmatrix}$$

$$W_i = \sum_{j=1}^{k} g_j V_{ij}$$

Simplifying equation (19) and using equations (17) and (18) yields

$$c_i = Q_i \left[\sum_{p=0}^{k} Q_p \right]^{-1} \tag{20}$$

where,

$$Q_o = \begin{vmatrix} q_{11} & q_{12} & \cdots & q_{1k} \\ q_{21} & q_{22} & \cdots & q_{2k} \\ \vdots & \vdots & \vdots & \vdots \\ q_{k1} & q_{k2} & \cdots & q_{kk} \end{vmatrix}, \quad Q_i = (-1)^i \begin{vmatrix} q_{01} & q_{02} & \cdots & q_{0k} \\ q_{11} & q_{12} & \cdots & q_{1k} \\ \vdots & \vdots & \vdots & \vdots \\ q_{(i-1)1} & q_{(i-1)2} & \cdots & q_{(i-1)k} \\ q_{(i+1)1} & q_{(i+1)2} & \cdots & q_{(i+1)k} \\ \vdots & \vdots & \vdots & \vdots \\ q_{k1} & q_{k2} & \cdots & q_{kk} \end{vmatrix}, \quad i = 1, 2, \ldots, k$$

Equation (20) gives the required controller design rules in terms of the transfer characteristics q_{oj} and q_{ij} $(i = 1,2,\ldots,k;\ j = 1,2,\ldots,k)$ of system models. The controller can thus be designed on-line by first estimating q_{oj} and q_{ij} using a suitable system identification algorithm and then using equation (20) to design the controller. The controller designed in this manner can easily be implemented on a digital processor and the

required control signals generated and applied in real-time. Moreover, to achieved on-line adaptation of the controller characteristics whenever a change in the system is sensed, a supervisory level control is required. The supervisor can be designed to monitor system performance and, based on a pre-specified quantitative measure of cancellation, initiate self-tuning control accordingly. In this manner, the actual cancellation achieved at the observation point can be measured, if this is within the pre-specified range then the controller will continue to process the detected signal, generate and output the cancelling signals. If the cancellation, however, is outside the specified limit then self-tuning will be initiated at the identification level. The self-tuning AVC algorithm can be outlined on the basis of the above as follows

(i) Switch off all secondary sources, estimate transfer functions q_{oj} $(j=1,2,\ldots,k)$.

(ii) Switch on secondary source i $(i=1,2,\ldots,k)$, estimate transfer functions q_{ij} $(j=1,2,\ldots,k)$.

(iii) Use equation (20) to obtain the transfer function of the controller c_i $(i=1,2,\ldots,k)$.

(iv) Implement the controller, to generate the control forces.

(v) Measure system performance and compare with pre-specified index, if within specified range then go to *(iv)* otherwise go to *(i)*.

The self-tuning AVC control system implemented according to the above algorithm is described in Figure 6, where 'plant' denotes the system in Figure 5 with the detected signal as the input and the observed signals as the outputs.

In implementing the self-tuning control algorithm described above, several issues of practical importance need to be given careful consideration. These include properties of the disturbance signal, robustness of the estimation and control, system stability and processor-related issues such as word length, speed and computational power.

The transfer functions q_{oj} and q_{ij} are represented in the discrete complex frequency (z) domain. Such a formulation also allows the corresponding time-domain representations of the system models in the form of difference equations. The RLS

algorithm used in the above utilises the difference equation representations with specified orders and, upon measurement of input/output signals of the system, produces parameters of the system model (Tokhi and Leitch, 1992). These parameters are used in steps *(i)* and *(ii)* above to obtain the corresponding transfer function representations of the models, q_{oj} and q_{ij}. The estimated transfer functions q_{oj} and q_{ij} thus obtained are used in equation (20) to obtain the required controller transfer functions c_i. These are then implemented in step *(iv)* above in the time domain using the corresponding difference equation representations.

In simulation experiments where the primary signal can be chosen properly to satisfy the robustness requirements of the control algorithm the problems due to the properties of the input signal will not arise. In practice, however, where the disturbance force may also excite those dynamics of the system which are not of interest, care must be taken to condition the input signal properly before sampling. Robustness of the control algorithm is related to the accuracy of the estimated plant model. This in turn depends on properties of input signal, proper initialisation of the parameter estimation algorithm, model order and accuracy of computation (Tokhi and Leitch, 1991a). The computational accuracy is related to the processor's dynamic range of computation, determined by the processor wordlength and type of arithmetic. With a processor supporting fixed-point arithmetic for example it is important to take necessary precautions against problems due to overflow and inaccuracies due to truncation/rounding of variables (Tokhi and Leitch, 1991a).

In employing the minimum variance design criterion, a problem commonly encountered is that of instability of system, specially, when non-minimum phase models are involved. Note in the controller design rules, equation (20), that such a situation will result in a non-minimum phase and unstable controller with the unstable poles approximately cancelling the corresponding zeros that are outside the stability region. Thus, to avoid this problem of instability either the estimated models can be made minimum-phase by reflecting their non-invertible zeros into the stability region and using the resulting minimum-phase models to design the controller or once the controller is designed the poles and zeros that are outside the stability region can be reflected into the stability region. In this manner, a factor $\left(1-pz^{-1}\right)$ corresponding to a pole/zero at $z=p$, in the complex

$z-$plane, that is outside the stability region can be reflected into the stability region by replacing the factor with $(p-z^{-1})$.

The supervisory level control described above is used as a performance monitor. In addition to monitoring system performance, it can also be facilitated with further levels of intelligence, for example, monitoring system stability and avoiding problems due to non-minimum phase models as describe above, verifying controller characteristics on the basis of practical realisation to make sure that impractically large controller gains are not required as discussed earlier, system behaviour in a transient period, model structure validation etc.

5 Implementations and results

To investigate the performance of the self-tuning AVC algorithm in broadband vibration suppression the beam simulation algorithm, as a test and evaluation platform, was implemented on the integrated DSP/transputer system using 20 grid-points along the beam. The self-tuning algorithm was first realised within a SISO control structure with the primary and secondary sources located at grid points 15 and 19 respectively, the detector at grid-point 15 and the observer at grid-point 11 along the beam. The self-tuning AVC algorithm was implemented on the integrated DSP-transputer system and its performance was assessed with a step disturbance force as the unwanted primary disturbance. Figure 7(a) shows the performance of the system as measured at the observation point, where $G_{D_o}(\omega)$ is the auto-power spectral density of the vibration signal before cancellation and $G_{oo}(\omega)$ is the corresponding autopower spectral density after cancellation. Figure 7(b) shows the difference $G_{D_o}(\omega)$-$G_{oo}(\omega)$, i.e. the actual attenuation. It is noted that, on average, about 25 dB cancellation is achieved over a broad range of frequencies of the disturbance covering the first five modes of vibration. The sharp dips noted in Figure 7(b), correspond to the resonance modes of vibration of the beam. Figure 8 shows the system performance over the lower frequency range covering the first two resonance modes of the beam. It is noted that, although the performance of the algorithm in broadband cancellation

is significant including the second and higher resonance modes, the amount of cancellation at the first resonance mode is of the order of five times lower than the overall average amount of cancellation achieved. However, it is seen from the corresponding time-domain description of the beam fluctuation before and after cancellation in Figure 9 that the level of unwanted disturbance is significantly reduced throughout the length of the beam. This is further evidenced in the corresponding frequency-domain description in Figure 10 given in terms of the average signal power throughout the length of the beam.

To investigate the performance of the self-tuning AVC algorithm within a SIMO control structure, a system with two secondary sources located at grid points 19 and 17, was realised. With the primary source and the detector both located at grid point 15, the self-tuning AVC system was implemented to achieve optimum cancellation at grid points 11 (observation point 1) and 9 (observation point 2). Figures 11, 12 and 13 show the performance of the system at the two observation points using a fixed disturbance force as the primary signal; the autopower spectral densities before cancellation, $G_{D_o}(\omega)$, and after cancellation, $G_{oo}(\omega)$, are shown in Figures 11 and 12 with the corresponding attenuations shown in Figure 13. It is seen that an average level of cancellation, over the broad frequency range of the disturbance, of at least 40 dB is achieved at each observation point. The sharp dips, noted earlier using the SISO controller as well, occur at the resonance frequencies of vibration of the beam. As compared with the performance of the system using the SISO controller in Figure 10, the amount of cancellation achieved at the lower resonance modes is significantly larger using the SIMO controller. Such a significant reduction in the level of the disturbance is reflected throughout the beam length as shown by the time-domain and corresponding frequency-domain descriptions of the beam behaviour before and after cancellation in Figures 14 and 15 respectively, where for visibility purposes the diagram in Figure 14(b) has been shown on a smaller vertical scale. It is noted from these results that the level of vibration is reduced by 95% throughout the beam length. This certainly demonstrates the capability of the self-tuning AVC algorithm in the suppression of vibration in flexible cantilever beam structures.

The control method developed aims at broadband vibration suppression. The transfer characteristics of the required controller, thus, designed and implemented are continuous frequency-dependent leading to a reduction of all the vibration modes of the structure. An important aspect of the design of the AVC system is the geometrical composition of system components. The stability of the system, due to the feedback loop(s) from the secondary source(s) to the detector, is affected by the location of the detector and secondary source(s) with respect to one another; if these are located so that the loop gain(s) at some frequency is unity then the system will be unstable. The detector in the system is used to gather information on the vibration modes of the system that need to be reduced. This information is then used to generate and apply the control force(s) through the secondary source(s). Thus, it is important to consider the location of the detector from the information gathering viewpoint and the secondary source(s) from the viewpoint of transfer of control energy into the vibration modes of the structure. In the case of the SISO control structure considered here the secondary source was placed at grid-point 19 where all the lower modes are principally dominant. This has resulted a reduction in the energy of all the lower modes at a similar level. However, when another secondary source is added at grid-point 17 where the first and second modes are more dominant than others, these two modes are reduced relatively more than the rest (see Figure 13). Note also that the energy transfer from grid-point 19 to the observation point at 12 or the observation point at 10 is less than that from grid-point 17 and the combined energy transfer from 17 and 19 is much more than that from 19 alone. Although, placing the secondary source in the SISO control structure at other locations may result in better performance, the results presented are aimed at demonstrating the performance of the single and multiple source AVC systems with nearly similar geometrical configurations.

A comparison of the performance of the system with the SIMO and SISO controllers is shown in Figure 16 in terms of the average signal power along the beam length before and after cancellation. It is clear from this diagram that the performance of the system with the SIMO controller is significantly better than that with the SISO controller. This implies that the utilisation of a multiple set of cancelling sources enhances the performance of the

system. However, it must be noted that the geometrical arrangement of system components as discussed earlier plays an important role in the performance of the system.

6 Conclusion

The design and implementation of a self-tuning AVC algorithm for flexible beam structures has been presented, discussed, and verified through numerical simulations. Active vibration control utilises the superposition of waves by artificially generating cancelling source(s) to destructively interfere with the unwanted source and thus result in cancellation. An active control mechanism for broadband cancellation of vibration of compact disturbance sources has been developed within an adaptive control framework. A supervisory level control has been incorporated within the control mechanism, allowing on-line monitoring of system performance and controller adaptation. The performance of the algorithm has been verified in the suppression of broadband vibration in a cantilever beam system within SISO and SIMO control structures. It is shown that, in employing the self-tuning control strategy, significant amounts of cancellation is achieved throughout the length of beam over the full frequency range of the disturbance.

7 Acknowledgements

Mr Hossain acknowledges the support of a research fellowship of the Association of Commonwealth Universities.

8 References

BAZ, A. and POH, S. (1988). "Performance of an active control system with piezoelectric actuators", Journal of Sound and Vibration, **126**, (2), pp. 327-343.

BAZ, A. and RO, J. (1991). "Active control of flow-induced vibrations of a flexible cylinder using direct velocity feedback", Journal of Sound and Vibration, **146**, (1), pp. 33-45.

BAZ, A., GILHEANY, J. and STEIMEJ, P. (1990a). "Active vibration control of propeller shafts", Journal of Sound and Vibration, **136**, (3), pp. 361-372.

BAZ, A., IMAM, K. and McCOY, J. (1990b). "Active vibration control of flexible beams using shape memory actuators", Journal of Sound and Vibration, **140**, (3), pp. 437-456.

BURTON, A. W. (1993). "Active vibration control in automotive chassis systems", IEE Computing and Control Engineering Journal, **4**, (5), pp. 225-232.

CHEN, L.-W. and KU, D.-M. (1990). "Dynamic stability analysis of a rotating shaft by finite element method", Journal of Sound and Vibration, **143**, (1), pp. 143-151.

FIROOZIAN, R. and STANWAY, R. (1988). "Active vibration control of turbomachinery: A numerical investigation of modal controllers", Mechanical Systems and Signal Processing, **2**, (3), pp. 243-264.

HARRIS, C. J. and BILLINGS, S. A. (1981). "Self-tuning and adaptive control: Theory and applications", Peter Peregrinus, London.

JAYASURIYA, S. and CHOPRA, S. (1990). "Active quenching of set of predetermined vibratory modes of a beam by a single fixed point actuator", International Journal of Control, **51**, (2), pp. 445-467.

KOURMOULIS, P. K. (1990). "Parallel processing in the simulation and control of flexible beam structure system", PhD. Thesis, Department of Automatic Control and Systems Engineering, The University of Sheffield, UK.

KRISHNAMURTHY, K. and CHAO, M.-C. (1992). "Active vibration control during deployment of space structures", Journal of Sound and Vibration, **152**, (2), pp. 205-218.

LEITCH, R. R. and TOKHI, M. O. (1987). "Active noise control systems", IEE Proceedings-A, 1987, **134**, (6), pp. 525-546.

LIN, Y.-H. and TRETHEWEY, M. W. (1990). "Finite element analysis of elastic beams subjected to moving dynamic loads", Journal of Sound and Vibration, **136**, (2), pp. 323-342.

LUEG, P. (1936). "Process of silencing sound oscillations", US Patent 2 043 416.

LU, J., CROCKER, M. J. and RAJU, P. K. (1989). "Active vibration control using wave control concepts", Journal of Sound and Vibration, **134**, (2), pp. 364-368.

TANAKA, N. and KIKUSHIMA, Y. (1988). "Rigid support active vibration isolation", Journal of Sound and Vibration, **125**, (3), pp. 539-553.

TOKHI, M. O. and LEITCH, R. R. (1991a). "Design and implementation of self-tuning active noise control systems", IEE Proceedings-D, **138**, (5), pp. 421-430.

TOKHI, M. O. and LEITCH, R. R. (1991b). "The robust design of active noise control systems based on relative stability measures", Journal of the Acoustic Society of America, **90**, (1), pp. 334-345.

TOKHI, M. O. and LEITCH, R. R. (1992). "Active noise control", Clarendon Press, Oxford.

TOKHI, M. O., VIRK, G. S. and HOSSAIN, M. A. (1992). "Integrated DSP^3 systems for adaptive active control", IEE Digest No. 1992/185: Colloquium on Active Techniques for Vibration Control Sources, Isolation and Damping, London, 28 October 1992, pp. 6/1-6/4

TZOU, H. S. and GADRE, M. (1990). "Active vibration isolation and excitation by piezoelectric slab with constant feedback gains", Journal of Sound and Vibration, **136**, (3), pp. 477-490.

TZOU, H. S. and TSENG, C. I. (1990). "Distributed piezoelectric sensor/actuator design for dynamic measurement/control of distributed parameter systems: A piezoelectric finite element approach", Journal of Sound and Vibration, **138**, (1), pp. 17-34.

UDUPA, K. M. and VARADAN, T. K. (1990). "Hierarchical finite element method for rotating beams", Journal of Sound and Vibration, **138**, (3), pp. 447-456.

VIRK, G. S. and KOURMOULIS, P. K. (1988). "On the simulation of systems governed partial differential equations", Proceedings of Control-88, Conference, pp. 318-321.

WELLSTEAD, P. E. and ZARROP, M. B. (1991). "Self-tuning systems - Control and signal processing", John Wiley, Chichester.

YANIV, O. and HOROWITZ, I. (1990). "Quantitative feedback theory for active vibration control synthesis", International Journal of Control, **51**, (6), pp. 1251-1258.

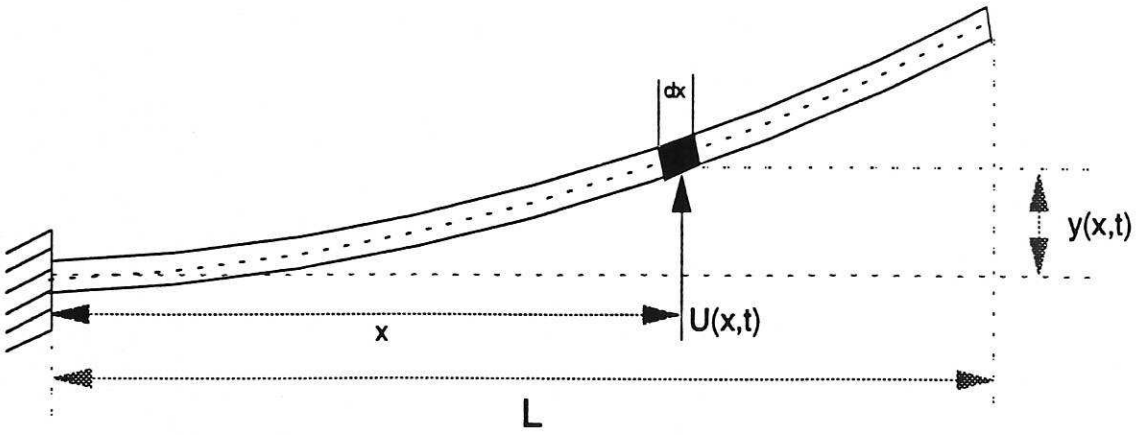

Figure 1: Schematic diagram of the cantilever beam system.

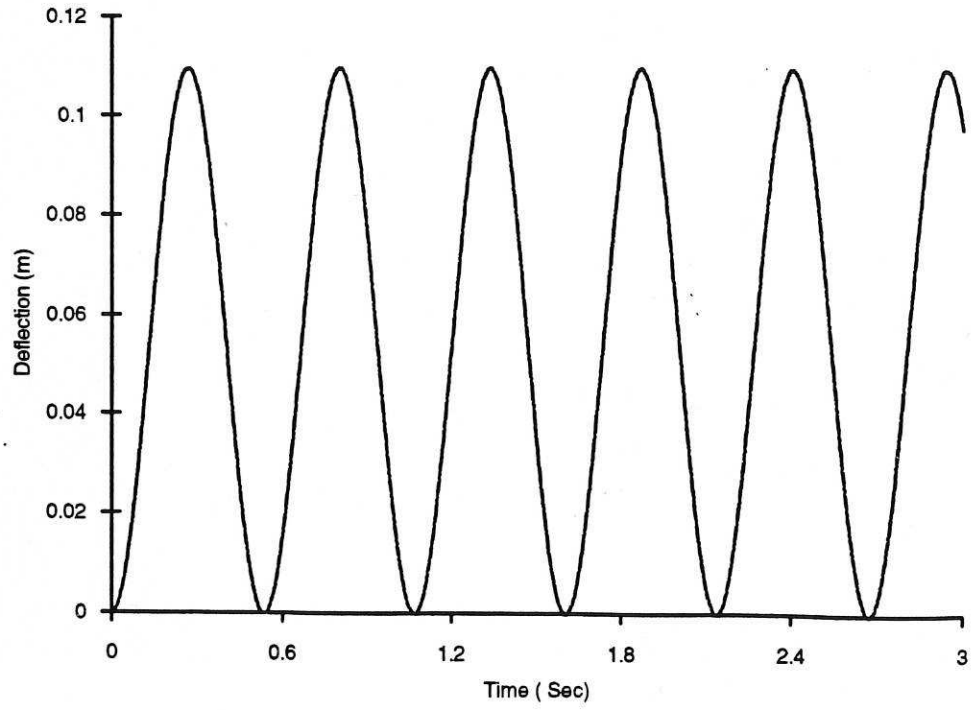

Figure 2: Step response of the beam at end-point.

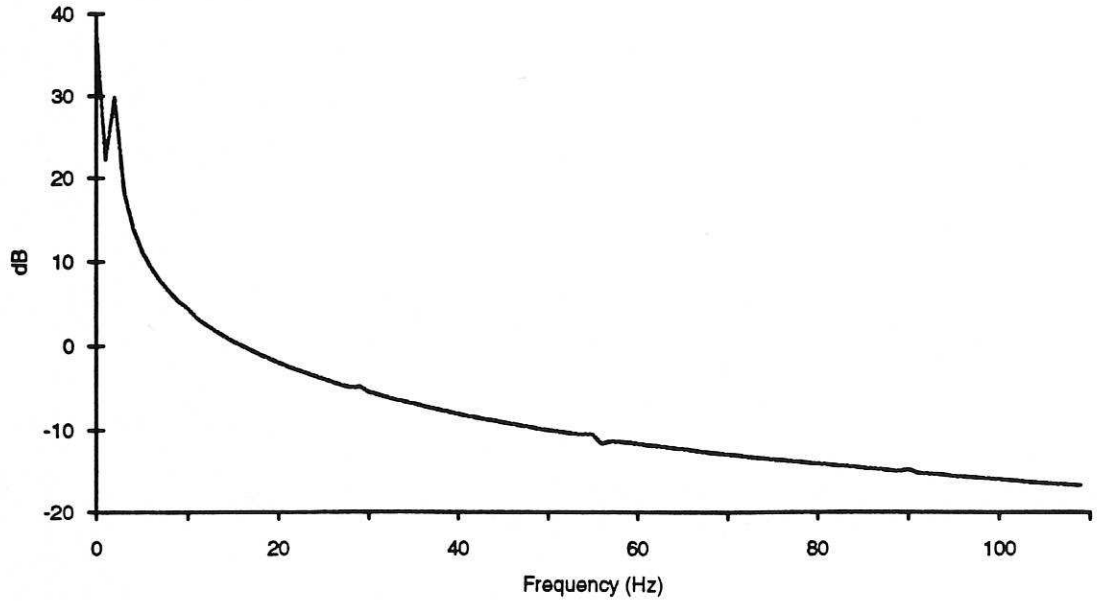

Figure 3: Autopower spectral density of step response of the beam at end-point.

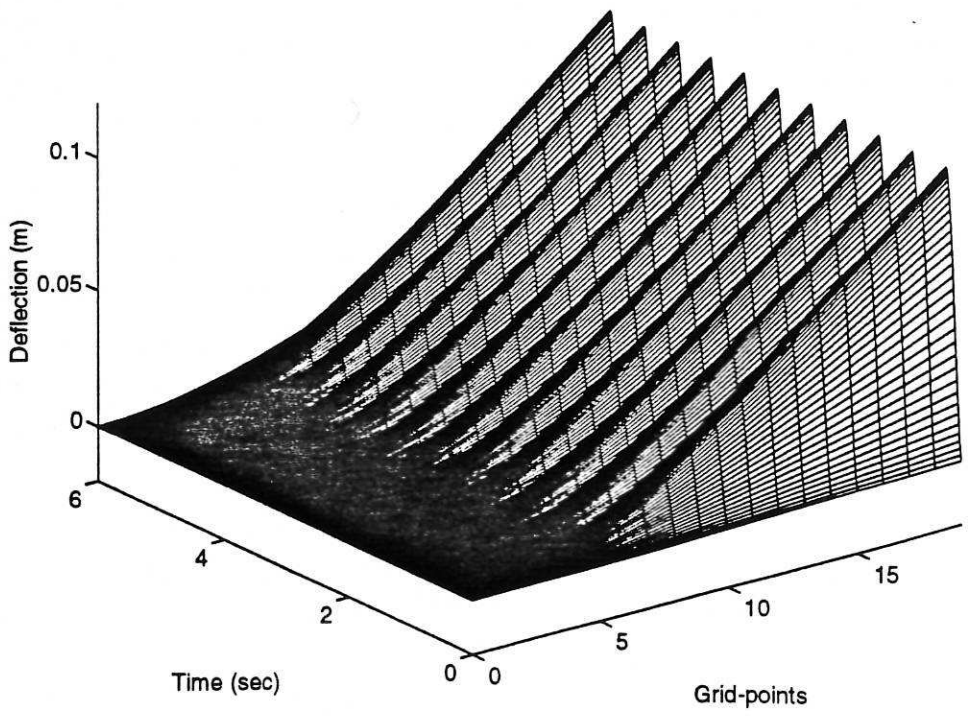

Figure 4: Step response of the beam along its length.

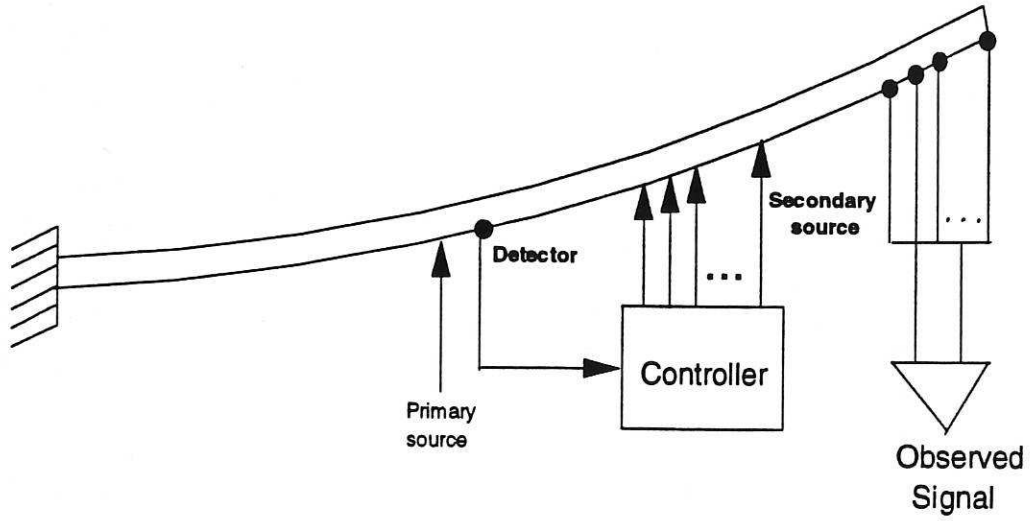

(a)

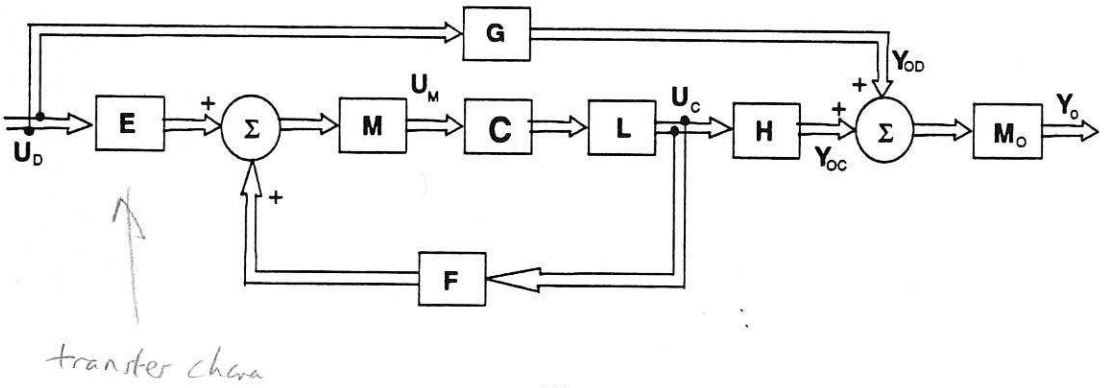

(b)

Figure 5: Active vibration control structure;
(a) Schematic diagram.
(b) Block diagram.

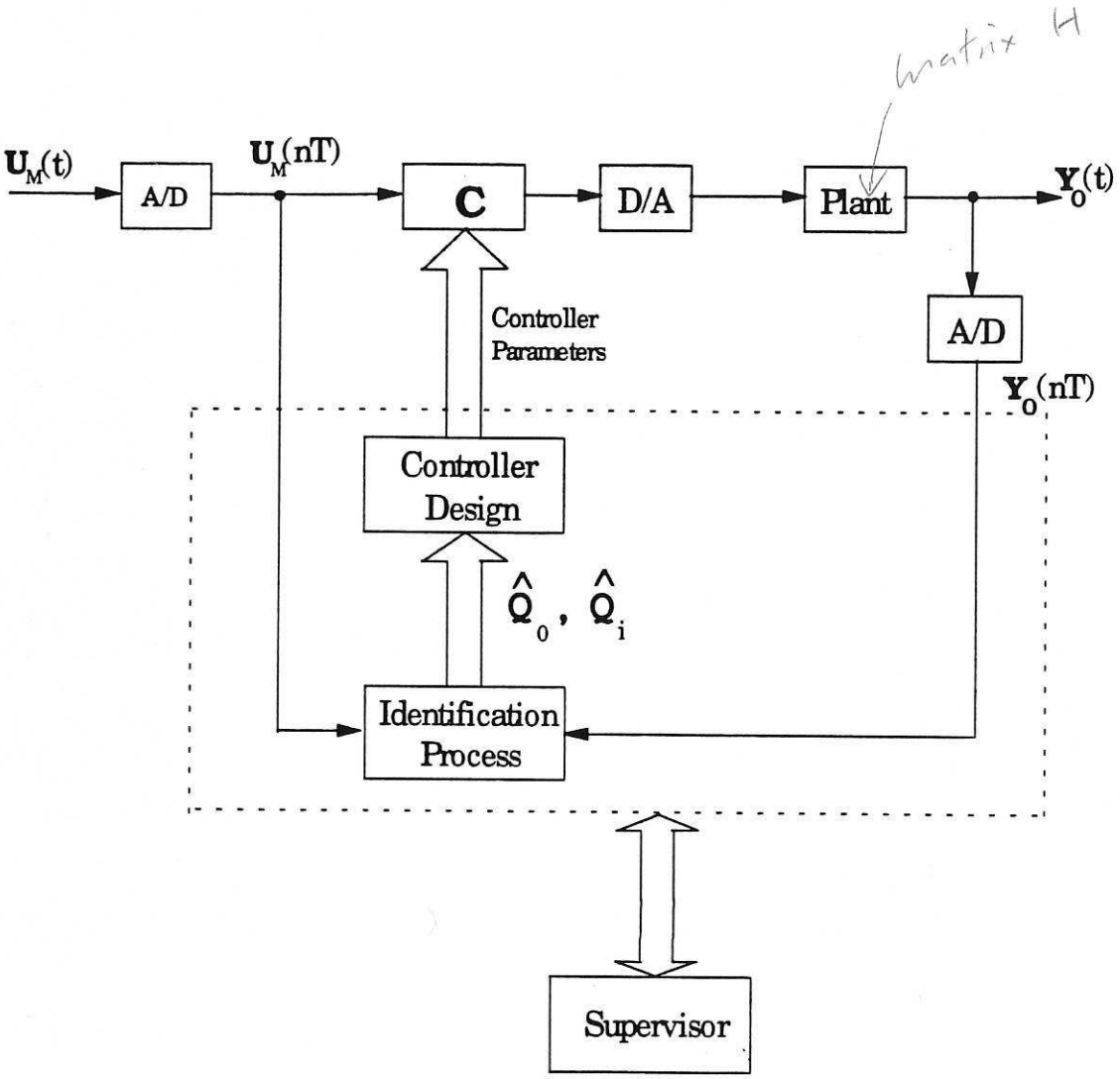

Figure 6: Self-tuning active vibration controller.

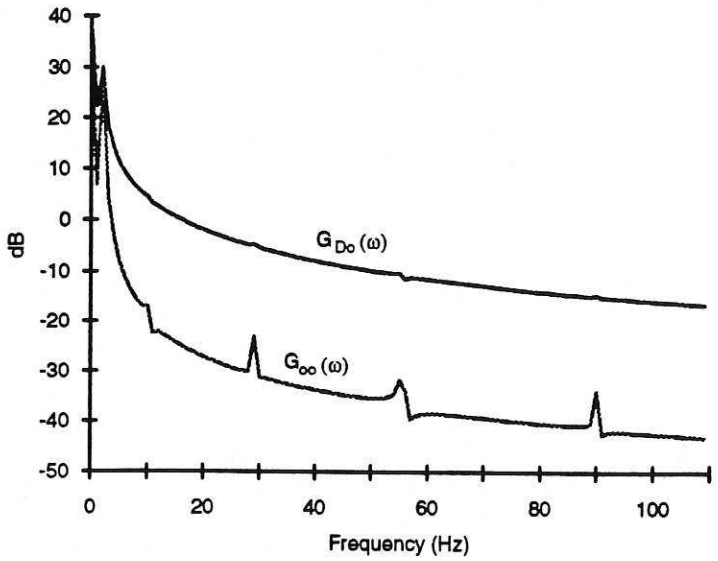

(a)

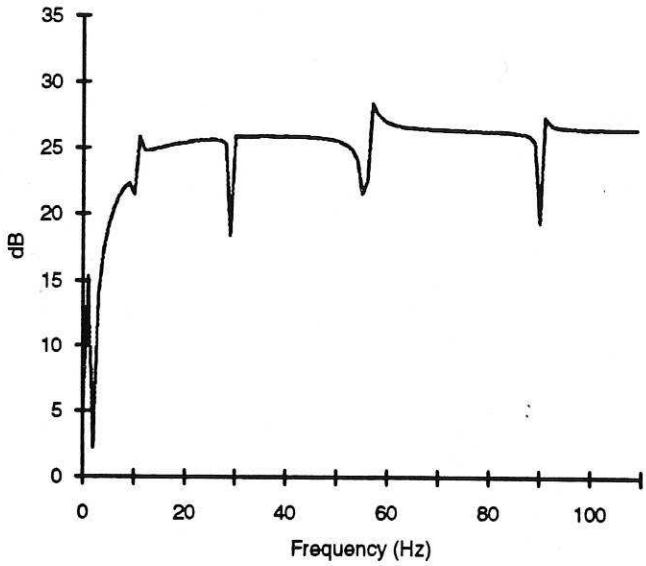

(b)

Figure 7: Performance of the SISO self-tuning AVC system at observation point;
(a) Spectral densities before and after cancellation.
(b) Attenuation in spectral density.

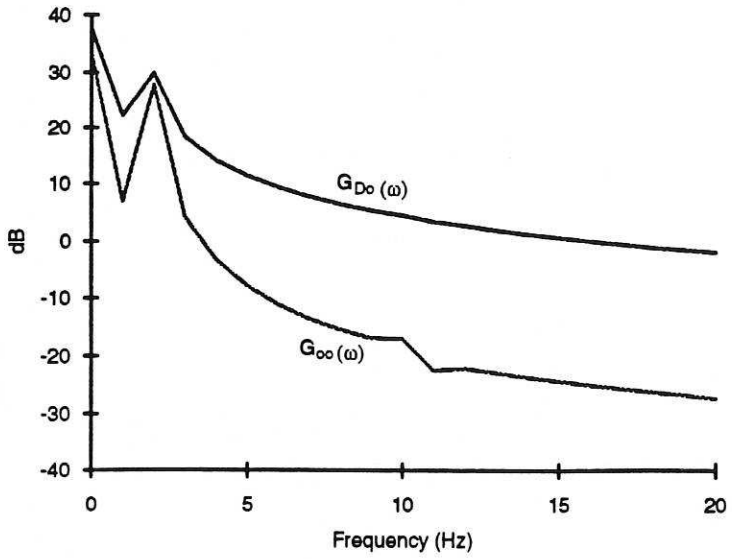

(a)

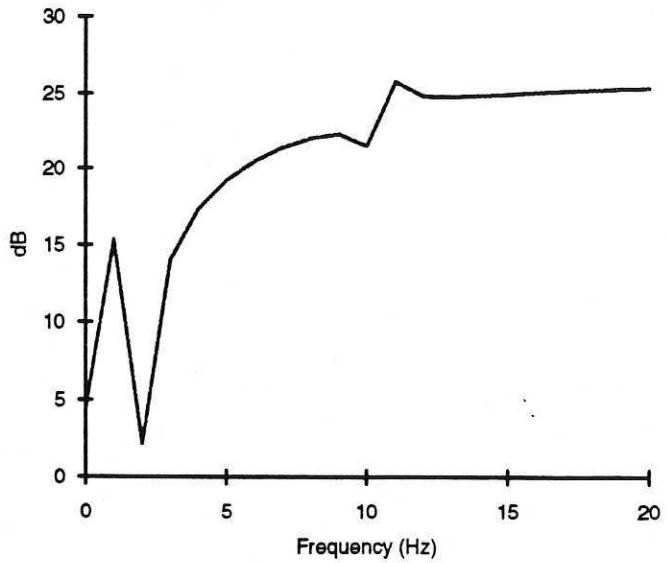

(b)

Figure 8: Performance of the SISO self-tuning AVC system at observation point;
(a) Spectral densities before and after cancellation.
(b) Attenuation in spectral density.

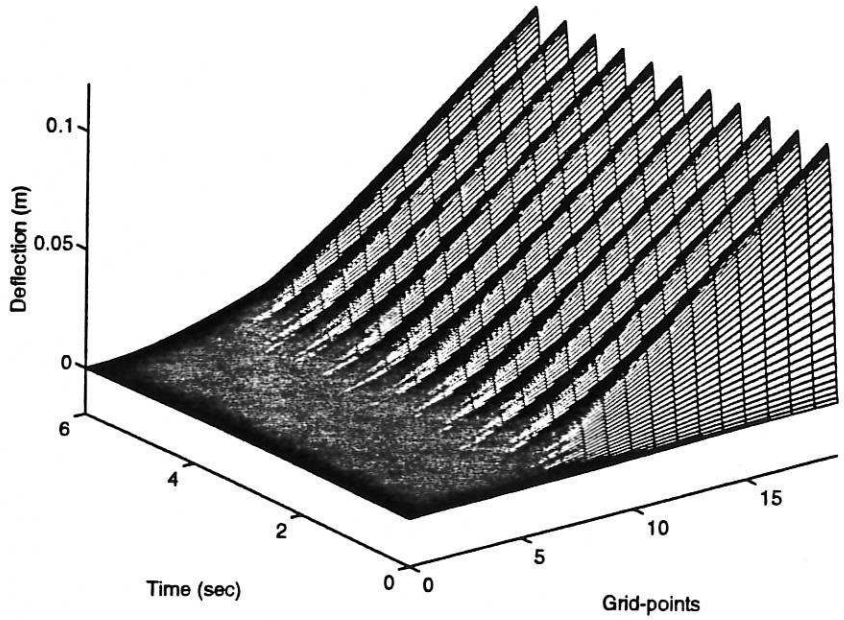

(a)

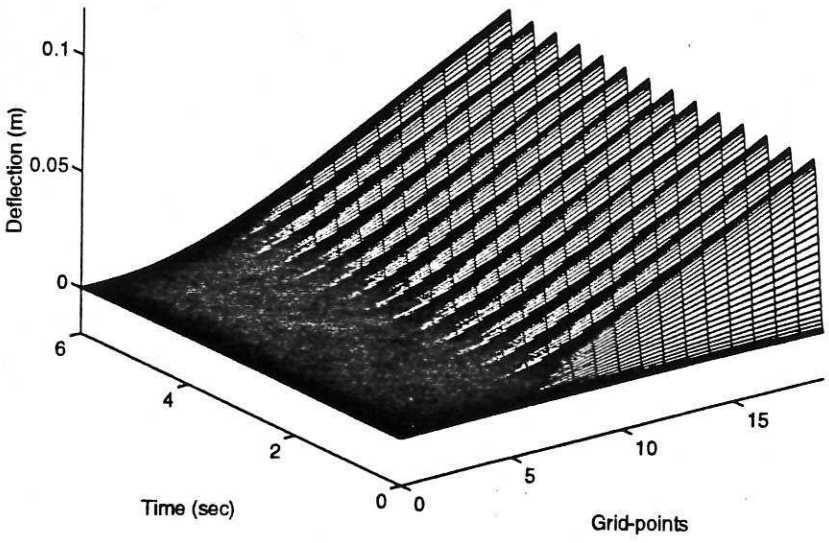

(b)

Figure 9: Performance of the SISO self-tuning AVC system along beam length;
(a) Beam fluctuation before cancellation.
(b) Beam fluctuation after cancellation.

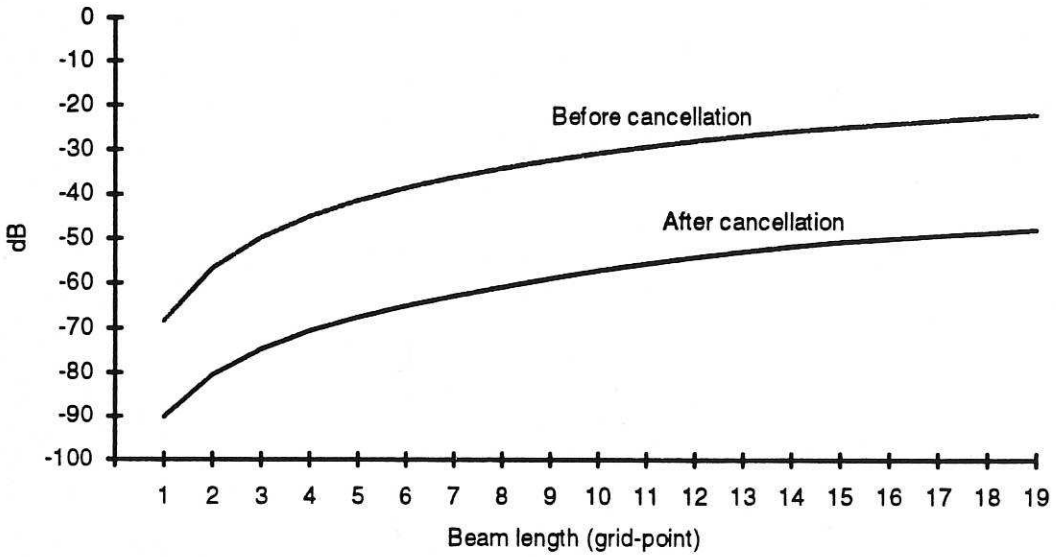

Figure 10: Average autopower spectral density of the disturbance along the beam before and after cancellation with the SISO self-tuning AVC system.

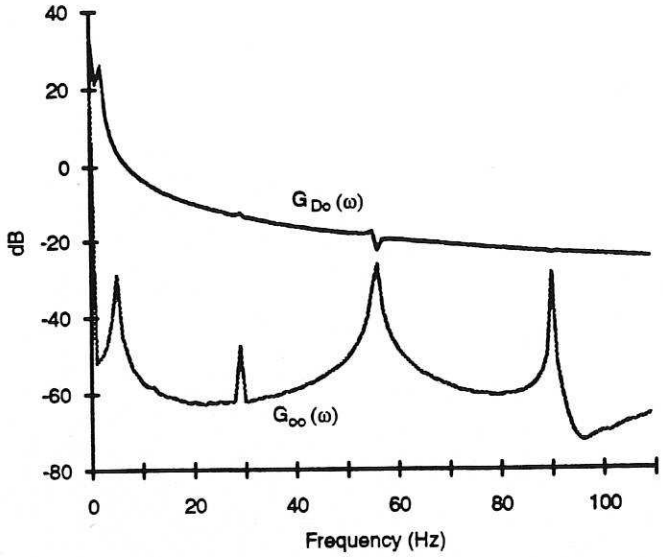

(a)

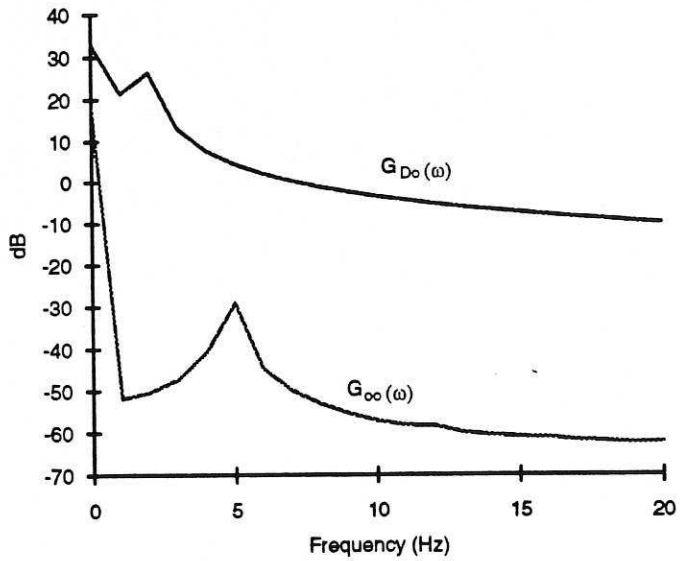

(b)

Figure 11: Autopower spectral density of the disturbance before and after cancellation with the SIMO self-tuning AVC system at observation point 1.

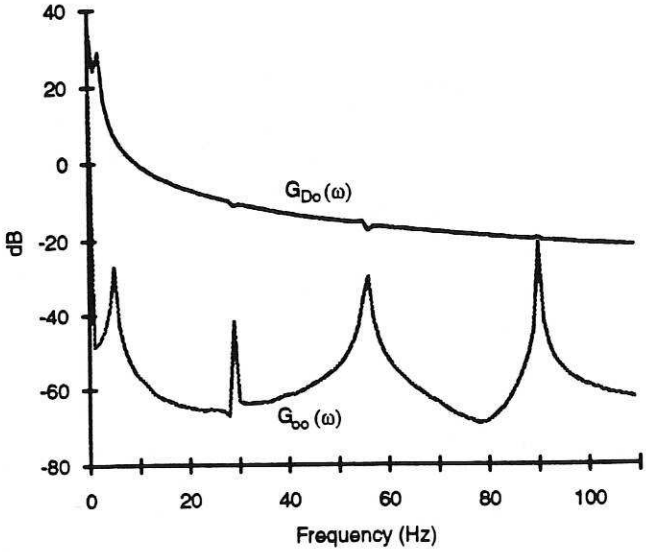

(a)

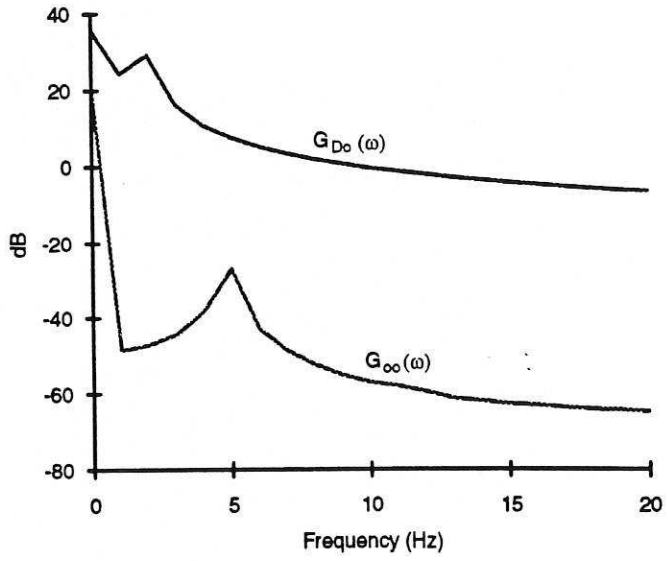

(b)

Figure 12: Autopower spectral density of the disturbance before and after cancellation with the SIMO self-tuning AVC system at observation point 2.

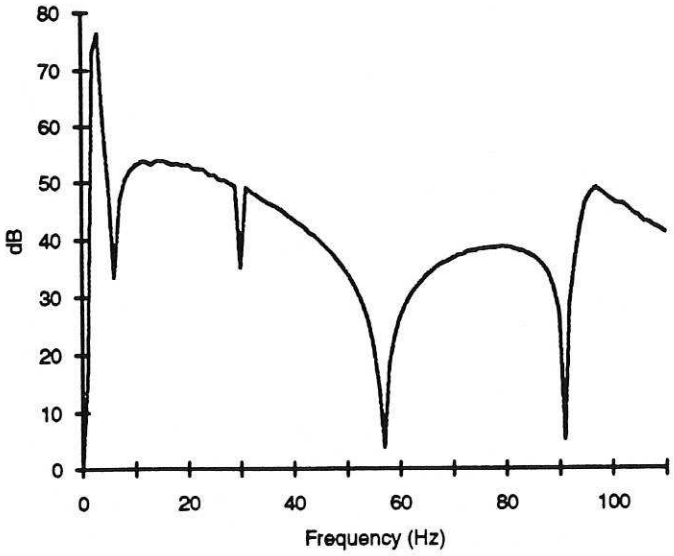

(a)

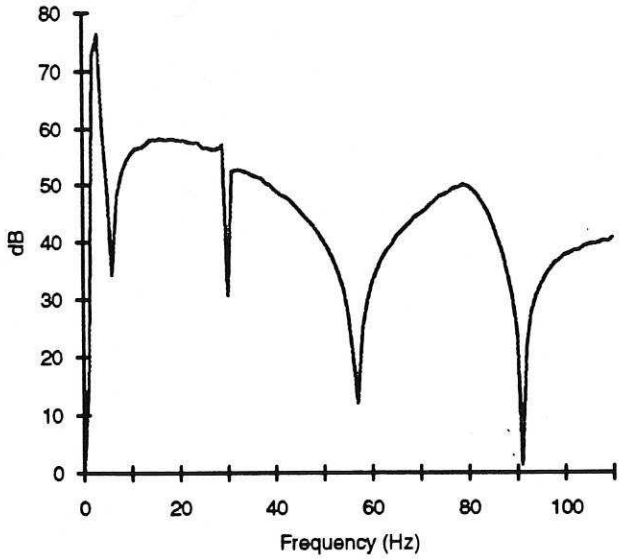

(b)

Figure 13: Attenuation in spectral density of the disturbance with the SIMO self-tuning AVC system;
(a) At observation point 1.
(b) At observation point 2.

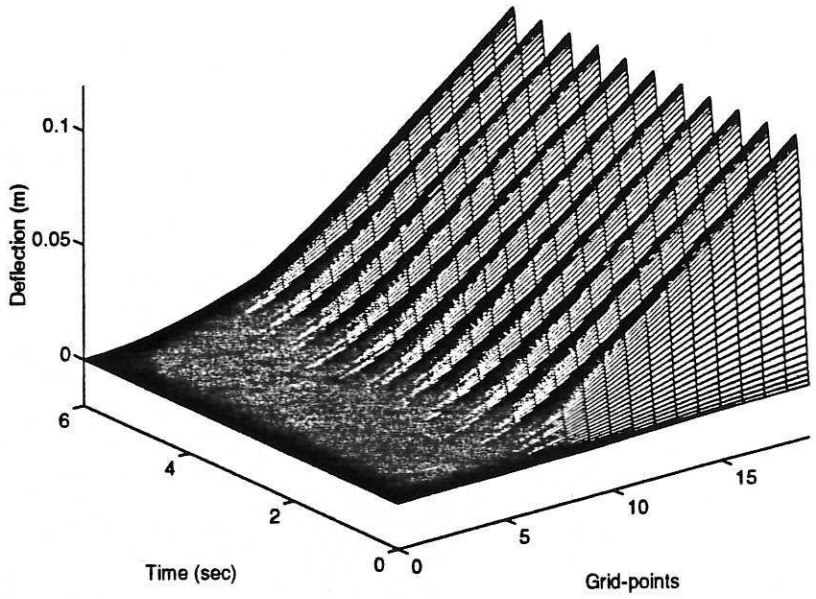

(a)

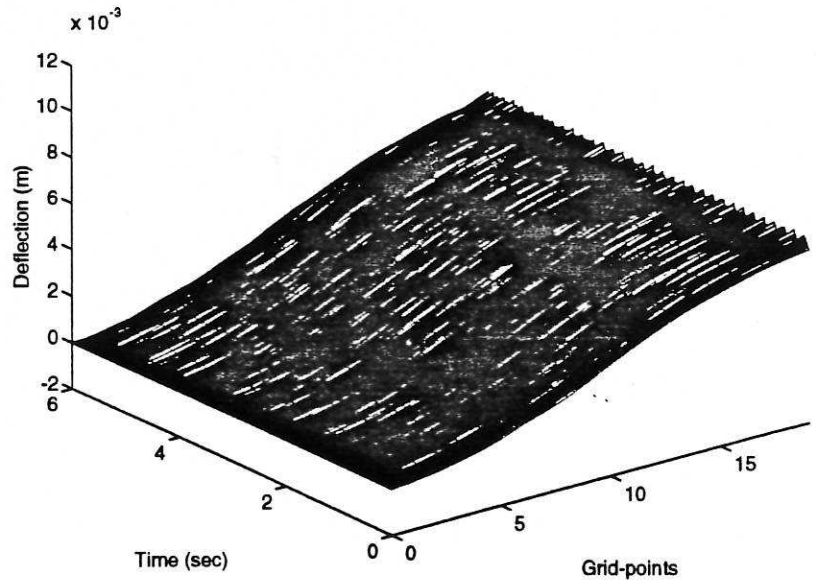

(b)

Figure 14: Performance of the of SIMO self-tuning AVC system along beam length;
(a) Beam fluctuation before cancellation.
(b) Beam fluctuation after cancellation.

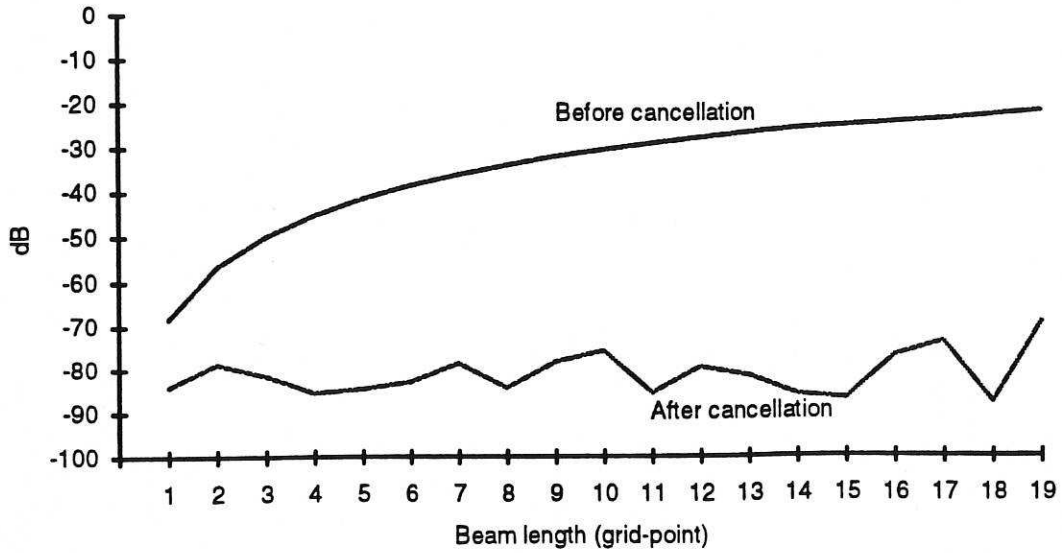

Figure 15: Average autopower spectral density of the disturbance along the beam before and after cancellation with the SIMO self-tuning AVC system.

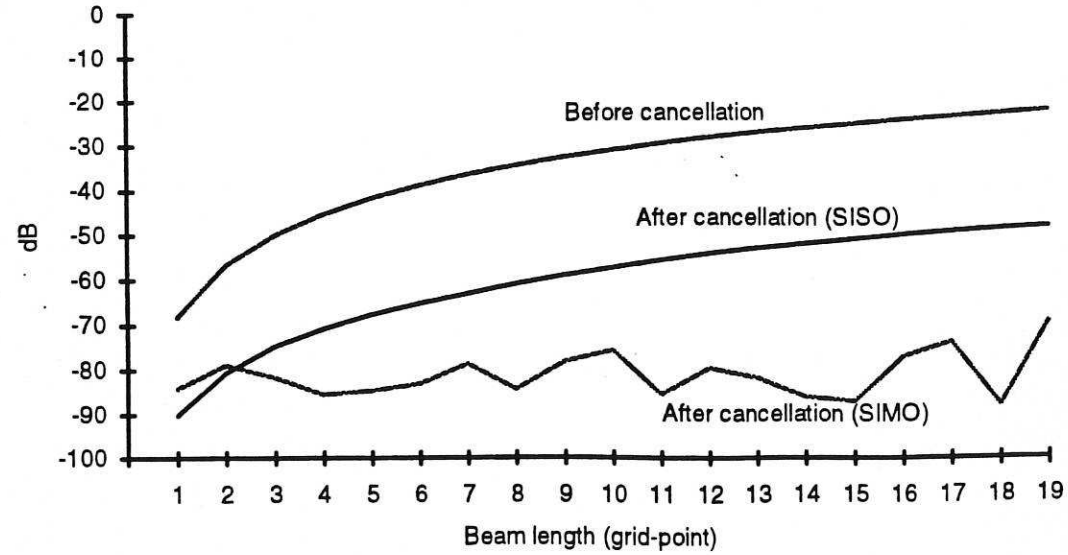

Figure 16: Average autopower spectral density of the disturbance along the beam before and after cancellation with the SISO and SIMO self-tuning AVC systems.